Materials Physics and Mechanics 44 (2020) 288-305 Received: July 29, 2019

AN APPROXIMATE ANALYTICAL SOLUTION FOR HYDRAULIC FRACTURE OPENING UNDER NON-UNIFORM INTERNAL PRESSURE

Kairui Li[1], N.N. Smirnov[1,2*], D.A. Pestov[1,2], Chengzhi Qi[3], A.B. Kiselev[1,2]

[1]Lomonosov Moscow State University, Leninskie Gory, 1, Moscow, 119991, Russia

[2]Scientific Research Institute for System Analysis of the Russian Academy of Sciences, Nakhimovskiy str. 36-1, Moscow, 117218, Russia

[3]Beijing High Institution Research Center for Engineering Structure and New Material, Beijing University of Civil Engineering and Architecture, Beijing, 100044, China

*e-mail: mech.math.msu@inbox.ru

Abstract. Because of the special non-uniform pressure distribution in hydraulic fracture, an especial hypothesis is proposed to get an approximate solution for the fracture opening, which satisfies the mixed boundary conditions on the fracture edges with the use of Bessel function integral properties. Error analysis of this approximate solution compared with the accurate solution is carried out. It is proved that the approximate solution is in good agreement with the accurate solution under the condition of this special pressure distribution in hydraulic-fracturing.

Keywords: hydraulic-fracturing, fracture opening, analytical solution, Bessel function

1. Introduction

With the development of the petroleum industry, hydraulic-fracturing technology is becoming increasingly important, in which one of the most important parameters is the fracture opening. Previously many inaccurate hypotheses were put forward for determination of the relationship between the fracture opening and the interior pressure, for example, the assumption of the uniform interior pressure distribution in the PKN model for hydraulic-fracturing [1,2] and the piecewise homogeneous hypothesis of the interior pressure distribution in the KGD model [3,4]. In recent time semi-analytical solution [5] and the discontinuous displacement method (DDM) [6] are applicated in many 2-dimensional or 3-dimensional simulations of hydraulic fracture growth [7-16] with the purpose of determination of the fracture opening on account of the interior non-uniform fluid pressure.

Based on the linear elastic fracture mechanics (LEFM) the solution for fracture opening

http://dx.doi.org/10.18720/MPM.4432020_2

under non-uniform interior fluid pressure was firstly obtained by I.N. Sneddon [5]. This solution represents a complex integral form that has singularities at some points. The main drawback of this solution is an inconvenience in applying at the actual oil production calculation or simulations of hydraulic-fracturing because of the complexity of the analytical solution type and the singularity at the fracture center [7-11]. Discontinuous displacement method (DDM) as the current popular numerical method in the fracture application is widely used in hydraulic-fracturing modeling [12-16], the essence of which lies in the fact that for only one fracture the fracture opening is obtained through the calculation of multi-dimensional linear equation system, the dimension of which depends on the grid number of this fracture. When many parallel fractures in the model, this means that the dimension of the linear equation system for the fracture opening becomes very large, and so the time and complexity of the calculation increase significantly.

The above analysis shows that traditional methods (analytical and numerical) are either complex or unsuitable for some especial situations in hydraulic-fracturing. Besides, for technology hydraulic-fracturing one approximate analytical solution for fracture opening that satisfies accuracy is relatively more applicable and more convenient than the semi-analytical solution and DDM. In this paper, we will try to find one simplified approximate analytical solution for fracture opening under non-uniform fluid pressure, which can satisfy the requirement of engineering accuracy and will be convenient for modeling calculation.

2. Mathematical model

On an infinite isotropic elastic plane there is a linear fracture with the length $2l$ along the axis x. The origin of coordinates is located at the fracture center (Fig. 1(a)), in which fluid moves from the center (the well) to the fracture tip to open the fracture and makes the fracture grow forward as a result of the non-uniform pressure $p(x)$.

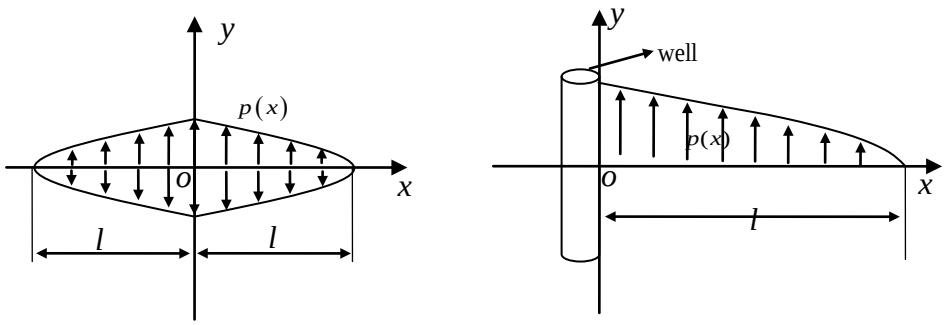

(a). The complete fracture model (b). The quarter structure of the fracture

Fig. 1. The classical fracture model

This model is a typical Griffith fracture model, so according to the theory of elasticity the equilibrium equations of this model in the condition of plane strain can be written:

$$\frac{\partial \sigma_x}{\partial x} + \frac{\partial \tau_{xy}}{\partial y} = 0,$$
$$\frac{\partial \tau_{xy}}{\partial x} + \frac{\partial \sigma_y}{\partial y} = 0. \tag{1}$$

The generalized Hooke's law:

$$\varepsilon_x = \frac{\partial u_x}{\partial x} = \frac{1+\nu}{E}[(1-\nu)\sigma_x - \nu\sigma_y],$$
$$\varepsilon_y = \frac{\partial u_y}{\partial y} = \frac{1+\nu}{E}[(1-\nu)\sigma_y - \nu\sigma_x], \tag{2}$$
$$\gamma_{xy} = 2\varepsilon_{xy} = \frac{\partial u_x}{\partial y} + \frac{\partial u_y}{\partial x} = \frac{2(1+\nu)}{E}\tau_{xy}.$$

The equations of deformation compatibility are yielded to only one equation for the 2-dimensional model:

$$\frac{\partial^2 \varepsilon_y}{\partial x^2} + \frac{\partial^2 \varepsilon_x}{\partial y^2} = \frac{\partial^2 \gamma_{xy}}{\partial x \partial y}, \tag{3}$$

where $\sigma_x, \sigma_y, \tau_{xy}$ are stress tensor components; $\varepsilon_x, \varepsilon_y, \gamma_{xy}$ are strain tensor components; u_x, u_y are deformation vector components, E is Young's modulus, and ν is Poisson's ratio.

Because of symmetry of the pressure distribution and symmetry of the fracture structure to axes x and y only the section $x \geq 0$ and $y \geq 0$ is taken into account for solving, see Fig. 1 (b), in which the following boundary conditions are satisfied:

$$\begin{aligned}
&x = 0, y > 0: && u_x = 0,\\
&\sqrt{x^2 + y^2} \to \infty: && \sigma_x = \sigma_y = \tau_{xy} = 0,\\
&y = 0, 0 < x < \infty: && \tau_{xy} = 0,\\
&y = 0, 0 \leq x \leq l: && \sigma_y = -p(x),\\
&y = 0, x > l: && u_y = 0.
\end{aligned} \tag{4}$$

3. Solution

A harmonic function $\Phi(x, y)$ is introduced in this model, which needs to satisfy:

$$\sigma_x = \frac{\partial^2 \Phi}{\partial y^2}, \quad \tau_{xy} = -\frac{\partial^2 \Phi}{\partial x \partial y}, \quad \sigma_y = \frac{\partial^2 \Phi}{\partial x^2}. \tag{5}$$

Combining equations (1), (2), (3), (5), we obtain:

$$\left(\frac{\partial^2}{\partial x^2} + \frac{\partial^2}{\partial y^2}\right)^2 \Phi = 0. \tag{6}$$

Since the stress component σ_y is symmetrical to axis x, it means that function $\Phi(x,y)$ is also symmetrical to axis x. Therefore, we can do the Fourier-cosine transform for the harmonic function $\Phi(x,y)$:

$$G(\omega,y)=\int_0^\infty \Phi(x,y)\cos(\omega x)dx, \tag{7}$$

where ω is a coefficient, and $\omega>0$. Its inverse transform:

$$\Phi(x,y)=\frac{2}{\pi}\int_0^\infty G(\omega,y)\cos(\omega x)d\omega. \tag{8}$$

Substituting equation (8) into equation (6),

$$\left(\frac{\partial^2}{\partial y^2}-\omega^2\right)^2 G=0. \tag{9}$$

According to the second boundary condition in equation (4): when $y\to\infty$, all stresses tend to zero. Therefore, the solution of equation (9) is needed to satisfy the following form:

$$G(y,\omega)=(A+By)e^{-\omega y}, \tag{10}$$

where coefficients A and B are functions of coefficient ω only.

Substituting equation (10) into the third boundary condition of equation (4),

$$\tau_{xy}|_{y=0}=-\omega\frac{\partial G}{\partial y}=-\omega e^{-\omega y}\left(B-A\omega-By\omega\right)|_{y=0}=0.$$

The relation of coefficients $A(\omega)$, $B(\omega)$ is obtained:

$$B=A\omega. \tag{11}$$

Taking advantage of this relationship stresses and strains can be expressed as follows:

$$\begin{aligned}
\sigma_x&=\frac{\partial^2\Phi}{\partial y^2}=\frac{2}{\pi}\int_0^\infty\left[A\omega^2(-1+\omega y)e^{-\omega y}\right]\cos(\omega x)d\omega,\\
\tau_{xy}&=-\frac{\partial^2\Phi}{\partial x\partial y}=-\frac{2}{\pi}\int_0^\infty \omega^3 Aye^{-\omega y}\sin(\omega x)d\omega,\\
\sigma_y&=\frac{\partial^2\Phi}{\partial x^2}=\frac{2}{\pi}\int_0^\infty -A\omega^2(1+\omega y)e^{-\omega y}\cos(\omega x)d\omega.
\end{aligned} \tag{12}$$

$$\begin{aligned}
u_x&=\frac{2(1+\nu)}{E\pi}\int_0^\infty A\omega(2\nu-1+\omega y)e^{-\omega y}\sin(\omega x)d\omega,\\
u_y&=\frac{2(1+\nu)}{E\pi}\int_0^\infty A\omega(2-2\nu+\omega y)e^{-\omega y}\cos(\omega x)d\omega.
\end{aligned} \tag{13}$$

According to the third and the fourth boundary conditions of equation (4), when $y=0$,

$$\sigma_y\,|_{y=0}=\frac{2}{\pi}\int_0^\infty -A\omega^2\cos(\omega x)d\omega=-p(x) \qquad 0\le x\le l,$$

$$u_y\,|_{y=0}=\frac{2(1+\nu)}{E\pi}\int_0^\infty A\omega(2-2\nu)\cos(\omega x)d\omega=0 \quad x>l.$$

After simplifying these above functions, a dual system of integral equations is obtained:

$$\begin{aligned}&\int_0^\infty A\omega^2\cos(\omega x)d\omega=-\frac{\pi}{2}p(x) \quad 0\le x\le l,\\&\int_0^\infty A\omega\cos(\omega x)d\omega=0 \qquad x>l.\end{aligned} \tag{14}$$

We know that the Bessel function has the following properties:

$$\begin{aligned}&\int_0^\infty J_1(\omega a)\cos(\omega x)\,d\omega=\begin{cases}\dfrac{1}{a}\left(1-\dfrac{x}{\sqrt{x^2-a^2}}\right) & x>a,\\ \dfrac{1}{a} & x\le a.\end{cases}\\&\int_0^\infty J_1(\omega a)\frac{\cos(\omega x)}{\omega}d\omega=\begin{cases}0 & x>a,\\ \dfrac{\sqrt{a^2-x^2}}{a} & x\le a,\end{cases}\end{aligned} \tag{15}$$

where a is a constant, x is the variable.

If fluid pressure in the fracture is a constant, namely uniform distribution: $p(x)=\tilde{p}$ is assumed, and the following assumption on A is valid:

$$A\omega^2=g\cdot J_1(\omega l), \tag{16}$$

where g is a coefficient to be determined, then substituting equation (16) into (14) we obtain:

$$\begin{aligned}&g\int_0^\infty J_1(\omega l)\cos(\omega x)d\omega=-\frac{\pi}{2}\tilde{p} \quad 0\le x\le l,\\&g\int_0^\infty J_1(\omega l)\frac{\cos(\omega x)}{\omega}d\omega=0 \qquad x>l.\end{aligned} \tag{17}$$

Using the results of equation (15) and letting $a=l$, the solution is easily found:

$$\begin{aligned}&g=-\frac{\pi l}{2}\tilde{p},\\&A\omega^2=-\frac{\pi l}{2}\tilde{p}J_1(\omega l).\end{aligned} \tag{18}$$

Substituting equation (18) into equation (13), the solution for the fracture opening is obtained:

$$w(x)=2u_y=\frac{4(1-\nu^2)}{E}\tilde{p}\sqrt{l^2-x^2}, \tag{19}$$

which is equal to the result in the article [5] when the pressure is uniformly distributed ($p(x)=\tilde{p}$). It means that this method for the solution of fracture opening is correct.

When the pressure distribution is non-uniform as it is in the actual situation, its special property of inhomogeneity was obtained in many articles [3,11,17-22] as shown in Fig. 2.

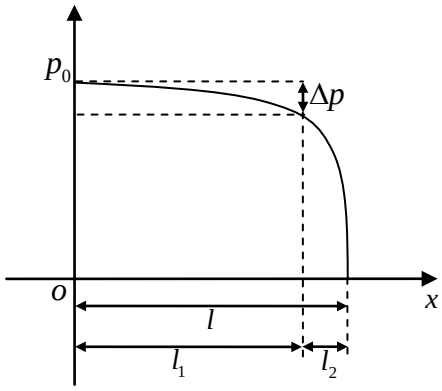

Fig. 2. The special non-uniform fluid pressure distribution in the plane-strain hydraulic fracture propagation

Fracture half-length l is split into two sections: (i) the first section $0 \sim l_1$, in which fluid pressure decreases very slowly along the axis x, namely the total pressure drop Δp in this section is very small compared with the fluid pressure in the well p_0; (ii) the second section $l_1 \sim l$, the length of this section l_2 is very small compared with the length of the first section l_1 and in this section, the fluid pressure decreases very quickly until equals to zero.

Because of the quite small values Δp and l_2 we can assume that the very slow decrease of fluid pressure in the first section ($0 \sim l_1$) and the very rapid decrease of fluid pressure in the second small section ($l_1 \sim l$) have little effect on the fracture opening, and the pressure distribution can be regarded as approximately homogeneous. Therefore, according to the analogy method, we can make the hypothesis in the actual situation of the inhomogeneous pressure similar to equation (16) in the ideal situation of uniform pressure:

$$A\omega^2 = g(x) \cdot J_1(\omega l), \tag{20}$$

where $g(x)$ is a coefficient function of x. The main purpose of introducing $g(x)$ is to satisfy the boundary condition of non-uniform pressure on the fracture edges, although it is not correct from the rigorous mathematical view. Later we will check the validity of this

hypothesis and whether it meets the requirement of engineering accuracy.

Substituting equation (20) into equation (14), we get

$$\begin{aligned} &g\int_0^\infty J_1(\omega l)\cos(\omega x)d\omega = -\frac{\pi}{2}p(x) \quad 0 \le x \le l, \\ &g\int_0^\infty J_1(\omega l)\frac{\cos(\omega x)}{\omega}d\omega = 0 \qquad\qquad x > l. \end{aligned} \tag{21}$$

Letting $a = l$ and substituting equation (15) into equation (21), we get

$$\begin{aligned} &g(x) = -\frac{\pi l}{2}p(x), \\ &A\omega^2 = -\frac{\pi l}{2}p(x)J_1(\omega l). \end{aligned} \tag{22}$$

Substituting solution (22) into expressions of stresses and displacements (12), (13), we get:

$$\begin{aligned} &\sigma_x = \frac{\partial^2\Phi}{\partial y^2} = -lp(x)\int_0^\infty\left[(-1+\omega y)e^{-\omega y}\right]J_1(\omega l)\cos(\omega x)d\omega, \\ &\tau_{xy} = -\frac{\partial^2\Phi}{\partial x\partial y} = lp(x)y\int_0^\infty J_1(\omega l)\omega e^{-\omega y}\sin(\omega x)d\omega, \\ &\sigma_y = \frac{\partial^2\Phi}{\partial x^2} = lp(x)\int_0^\infty J_1(\omega l)(1+\omega y)e^{-\omega y}\cos(\omega x)d\omega. \end{aligned} \tag{23}$$

$$\begin{aligned} &u_x = \frac{(1+\nu)}{E}lp(x)\int_0^\infty J_1(\omega l)(2\nu-1+\omega y)e^{-\omega y}\frac{\sin(\omega x)}{\omega}d\omega, \\ &u_y = \frac{(1+\nu)}{E}lp(x)\int_0^\infty J_1(\omega l)(2-2\nu+\omega y)e^{-\omega y}\frac{\cos(\omega x)}{\omega}d\omega. \end{aligned} \tag{24}$$

And then substituting the results (23), (24) into equation (4) to recheck the boundary conditions, we get:

$$\begin{aligned} &x = 0,\ y > 0: \quad u_x = 0, \\ &\tau_{xy}|_{y=0} = lp(x)y\int_0^\infty J_1(\omega l)\omega e^{-\omega y}\sin(\omega x)d\omega = 0 \quad 0 \le x \le \infty, \\ &\sigma_y|_{y=0} = lp(x)\int_0^\infty J_1(\omega l)\cos(\omega x)d\omega = -p(x) \qquad 0 \le x \le l, \\ &u_y|_{y=0} = \frac{2(1-\nu^2)}{E}lp(x)\int_0^\infty J_1(\omega l)\frac{\cos(\omega x)}{\omega}d\omega = 0 \quad x > l. \end{aligned}$$

All boundary conditions are satisfied. Therefore, when $y = 0$, $0 \le x \le l$ the displacement of the fracture edge is obtained:

$$u_y = \frac{2(1-\nu^2)}{E}p(x)\sqrt{l^2-x^2}. \tag{25}$$

And the fracture opening:

$$w(x) = 2u_y = \frac{4(1-\nu^2)}{E} p(x)\sqrt{l^2 - x^2}. \tag{26}$$

3. Comparative analysis of the approximate solution

The most well-known semi-analytical solution for fracture opening under non-uniform pressure was obtained by I.N. Sneddon [5]:

$$w(x) = \frac{4(1-\nu^2)}{E\pi}\int_0^l p(x)\ln\left|\frac{\sqrt{l^2-x^2}+\sqrt{l^2-\zeta^2}}{\sqrt{l^2-x^2}-\sqrt{l^2-\zeta^2}}\right| d\zeta. \tag{27}$$

Due to the appearance of a special integral in this solution, a complete analytical solution cannot be obtained, and when applied in numerical simulation or engineering calculation this solution is singular at some points. Moreover, the essence of the integral is the summation of all divided fracture segments as the method DDM, which spends a lot of computation time.

Below the approximate solution (26) in this paper and the semi-analytical solution (27) will be compared and analyzed according to the results in articles [20,22], which were obtained through accurate numerical modeling and self-similar solution of hydraulic fracturing process:

$$\begin{aligned} p(x,t) &= \frac{\mu'^{1/3}E'^{2/3}}{t^{1/3}}\left[\Pi_0(\xi)+\varepsilon(\kappa)\Pi_1(\xi)\right], \\ l(t) &= \frac{Q_0^{1/2}E'^{1/6}t^{2/3}}{\mu'^{1/6}}\left[\gamma_0+\varepsilon(\kappa)\gamma_1\right]. \end{aligned} \tag{28}$$

Here, $E' = \frac{E}{1-\nu^2}, \mu' = 12\mu$ (μ is the fluid viscosity), t is injection time, Q_0 is the injection fluid velocity, $K' = 4\left(\frac{2}{\pi}\right)^{1/2} K_{Ic}$ (K_{Ic} is the rock toughness), $\gamma_0 \approx 0.61524$, $\gamma_1 \approx -0.1753$, $\varepsilon(\kappa) = B_1\kappa^b$ ($\kappa = \frac{K'}{E'}\left(\frac{E'}{\mu' Q_0}\right)^{1/4}$, $B_1 \approx 0.1076$, $b \approx 3.16796$), and the dimensionless functions $\bar{\Omega}_0(\xi), \bar{\Omega}_1(\xi), \Pi_0(\xi), \Pi_1(\xi)$ are in following forms:

$$\begin{aligned} \bar{\Omega}_0(\xi) &= a_{01}(1-\xi^2)^{2/3} + a_{02}(1-\xi^2)^{5/3} + a_{03}\left[2(1-\xi^2)^{1/2} + \xi^2\ln\left|\frac{1-(1-\xi^2)^{1/2}}{1+(1-\xi^2)^{1/2}}\right|\right], \\ \Pi_0 &= b_{01}\,{}_2F_1\left(-\frac{1}{6},1,\frac{1}{2},\xi^2\right) + b_{02}\,{}_2F_1\left(-\frac{7}{6},1,\frac{1}{2},\xi^2\right) + b_{03}\left(2-\pi|\xi|\right). \end{aligned} \tag{29}$$

$$\bar{\Omega}_1(\xi)=a_{11}\left(1-\xi^2\right)^h+\left(a_{12}+a_{13}\xi^2\right)\left(1-\xi^2\right)^{1+h}+$$
$$+a_{14}\left[2\left(1-\xi^2\right)^{1/2}+\xi^2\ln\left|\frac{1-\left(1-\xi^2\right)^{1/2}}{1+\left(1-\xi^2\right)^{1/2}}\right|\right],$$
$$\Pi_1(\xi)=b_{11}\,{}_2F_1\left(c_{11},1,\frac{1}{2},\xi^2\right)+b_{12}\,{}_2F_1\left(c_{12},1,\frac{1}{2},\xi^2\right)\xi^2+b_{13}\,{}_2F_1\left(c_{13},2,\frac{3}{2},\xi^2\right)+$$
$$+b_{14}\left(2-\pi|\xi|\right), \tag{30}$$

where coefficients $\xi=\frac{x}{l}$, $a_{01}\approx 1.73205$, $a_{02}\approx -0.15601$, $a_{03}\approx 0.13264$, $b_{01}\approx 0.475449$, $b_{02}\approx -0.061178$, $b_{03}\approx 0.066322$, $a_{11}\approx 0.908354$, $a_{12}\approx 0.025574$, $a_{13}\approx -0.083814$, $a_{14}\approx -0.09095$, $b_{12}\approx 0.017132$, $b_{13}\approx -0.039015$, $b_{14}\approx -0.045476$, $c_{11}\approx 0.36133$, $c_{12}\approx -1.63867$, $c_{13}\approx -0.638673$, and ${}_2F_1(\cdot,\cdot,\cdot,\cdot)$ is Gauss's hypergeometric function.

We select the different cases for comparison, which are characterized by different pressure distribution under different model coefficients of the fluid, rock characteristics, and the injection conditions. The first case for comparison: we select three different pressure distributions in the fracture with the same length ($l=7\ m$), shown in Fig. 3, in which p_0 represents the maximum pressure in the fracture, namely the well pressure. The second case: comparison is performed for different fracture length under the same well pressure p_0, which is shown in Fig. 4. The third case: comparison is provided for the different pressure distributions in different time moments, which means the fracture length and the well pressure p_0 are different from others (see Fig. 5).

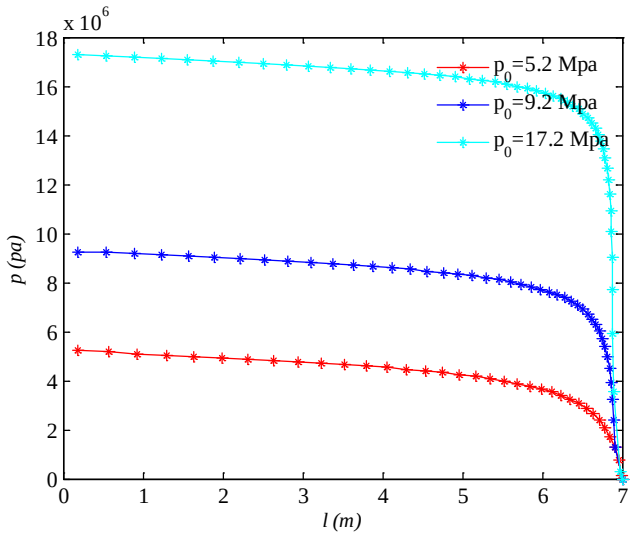

Fig. 3. The different pressure distributions with the same fracture length ($l=7\ m$)

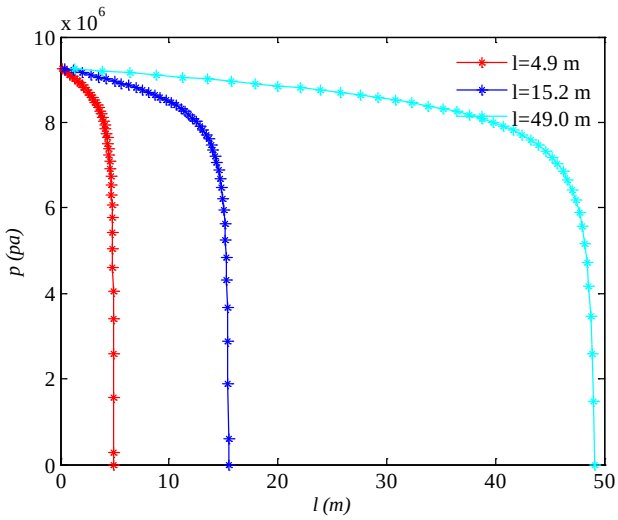

Fig. 4. The different pressure distributions with the same well pressure ($p_0 = 9.2\ MPa$) and different fracture lengths

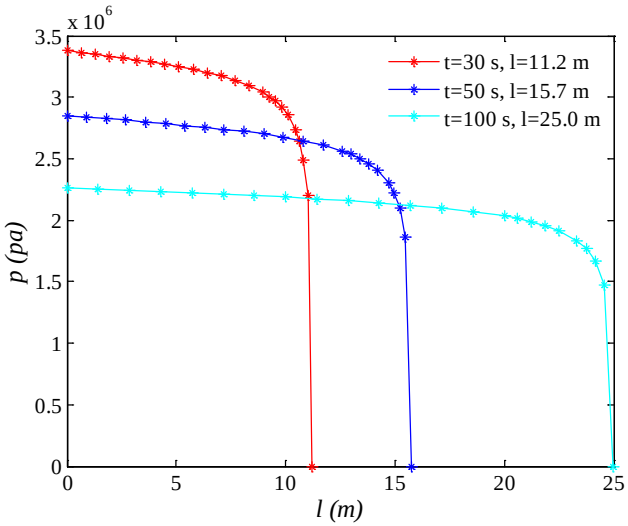

Fig. 5. The different pressure distributions with the different well pressure and different fracture lengths under the different time

4. Results of comparative analysis

Results of the first case of comparative analysis. According to the formulas (26), (27) and data in Fig. 3 the respective fracture openings can be obtained, which are shown in Figs. 6, 7, 8.

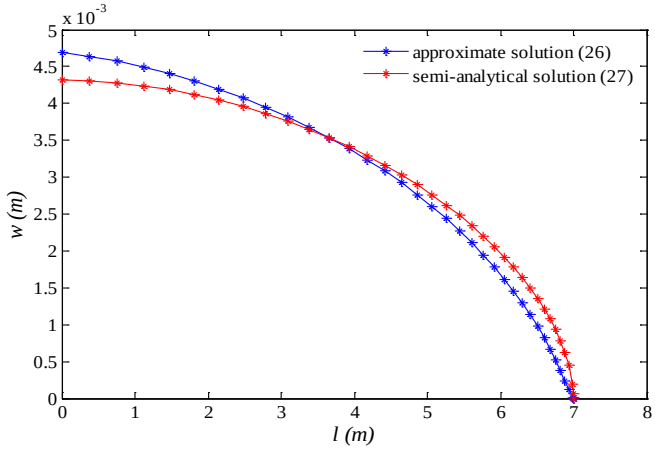

Fig. 6. The fracture openings from the approximate and semi-analytical solutions under p_0=5.2 *MPa*

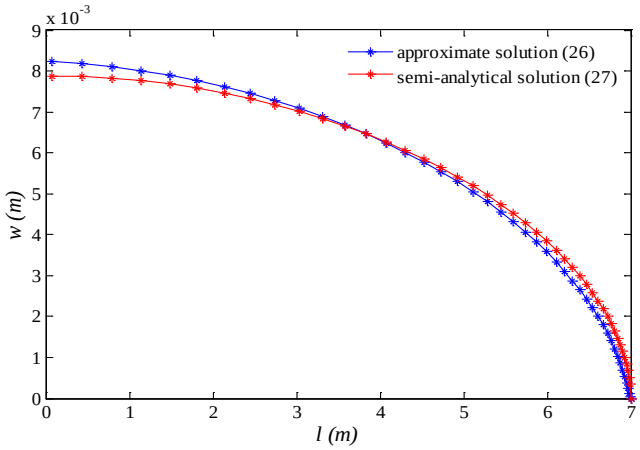

Fig. 7. The fracture openings from the approximate and semi-analytical solutions under p_0=9.2 *MPa*

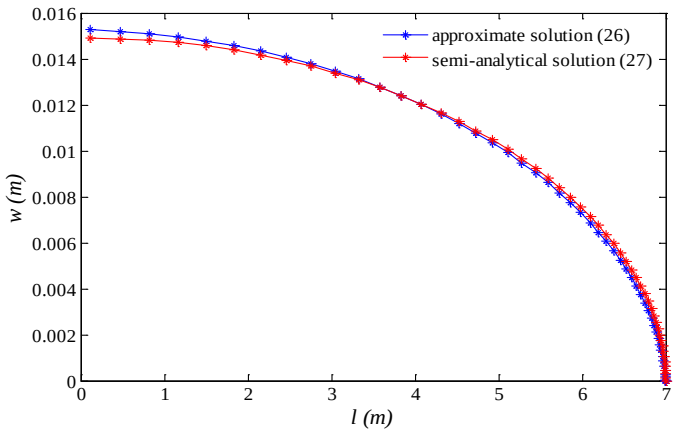

Fig. 8. The fracture openings from the approximate and semi-analytical solutions under p_0=17.2 *MPa*

From Figures 6, 7, 8 it is found that near the well values from the solution (26) are slightly larger than values from the semi-analytical solution (27); near the middle of half-fracture values from the two solutions are the same, then close to the tip of the fracture, values from the solution (26) are slightly smaller than values of the solution (27). In general, the approximate solution (26) coincides with the semi-analytical solution (27) very well, moreover, with the increase of the well pressure the difference between the approximate solution (26) and the semi-analytical solution will get smaller and smaller. The approximate solution can serve a good approximation for actual underground oil extraction simulation, because the in-situ stresses are very big (usually greater than $17.2\ MPa$), which means that in actual situation equation (26) is suitable for engineering calculation.

Here we define a new variable, which is called relative error of fracture opening for every point along the fracture with the expression:

$$\varepsilon_i = \left| \frac{w_i - w_i^*}{w_0^*} \right|, \tag{31}$$

where w_i is the approximate value of fracture opening from solution (26) at the i point; w_i^* represents the accurate value of fracture opening from solution (27) at the same point; w_0^* is the accurate value of fracture opening at the center of the fracture from the solution (27).

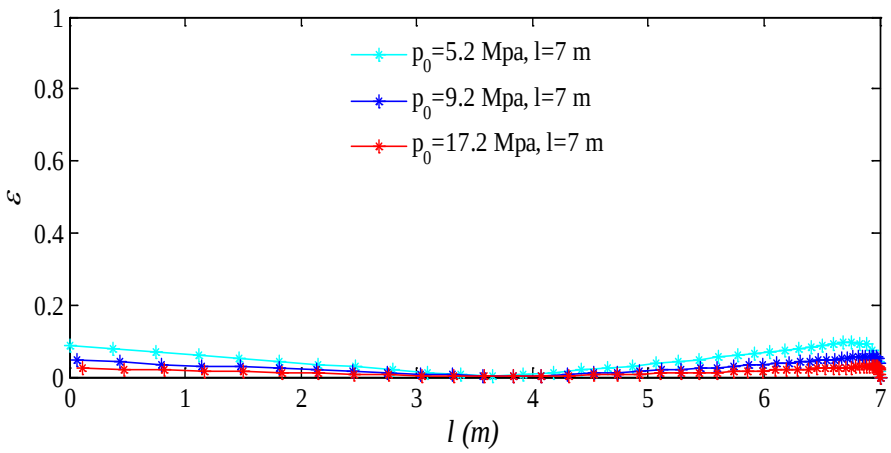

Fig. 9. The relative errors for the three different pressure distributions in Fig. 3

Figure 9 shows that the relative errors monotonously decrease, equal to zero near the middle of the half-fracture, and then monotonously increase, near the tip of fracture quickly decreases. Besides, it is shown that the solution (26) comes closer to the accurate semi-analytical solution (27) as the well pressure p_0 increases. The most important is that the maximum of the relative errors is less than 0.1, which means that the solution (26) is very

close to the solution (27).

Results of the second case of comparative analysis. As similar to section 4.1, the results of the second case of comparative analysis (see Fig. 4) are shown in Fig. 10, 11, 12, respectively. We can find that in general, the solution (26) tends to be very close to the exact solution (27). Approximately before the middle of the half-fracture, the solution is slightly larger than the solution (27) and there is an inverse characteristic after the middle of the fracture.

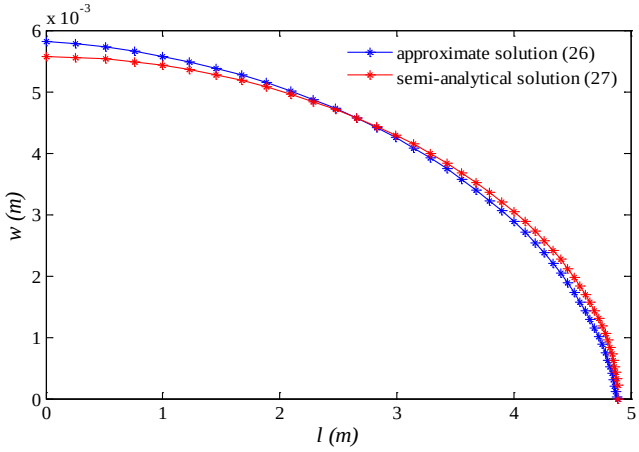

Fig. 10. The fracture openings from the approximate and semi-analytical solutions under l=4.9 m

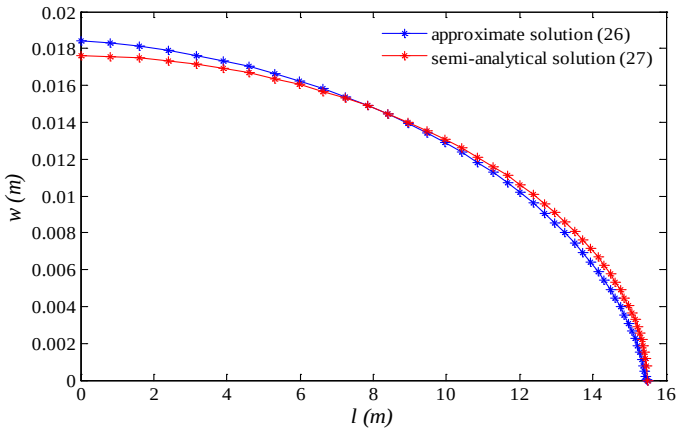

Fig. 11. The fracture openings from the approximate and semi-analytical solutions under l=15.2 m

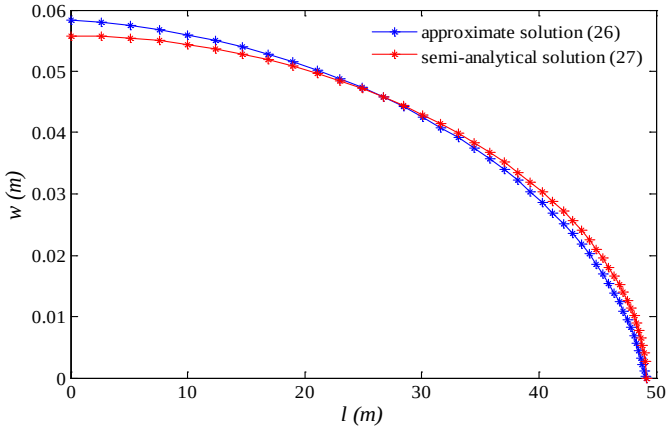

Fig. 12. The fracture openings from the approximate and semi-analytical solutions under l=49.0 m

According to the definition in equation (31), relative errors can be obtained, which are shown in Fig. 13. In general, the results obtained from solution (26) for three situations (in Fig. 4) coincide very well ($\varepsilon_i \ll 0.1$) with the results from the solution (27). The tendency of this contrast form is the same as the tendency of the first contrast form in section 4.1. It should be noted that approximately after the middle of the half-fracture the relative errors begin to increase, and close to the end of the fracture decrease rapidly to zero. Despite the occurrence of this characteristic at the end of the fracture, the accuracy of the equation (26) cannot be affected.

Besides, it is also found that as the length of fracture increases, the relative errors become smaller and smaller. It means that solution (26) is getting closer and closer to the accurate solution (27) when the fracture grows forward.

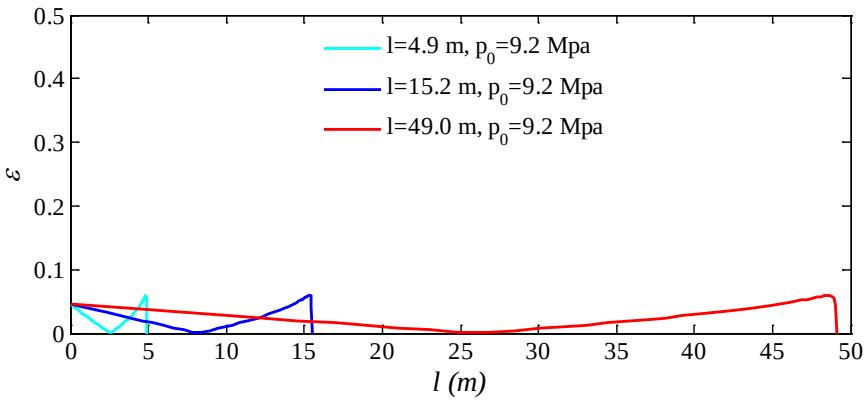

Fig.13. The relative errors of the above three different pressure distributions in Fig. 4

Results of the third case of comparative analysis. According to the pressure distribution in Fig. 5 the comparative analysis results including the relative errors are shown in Figs. 14, 15, 16, and 17. The final result in this form is the same as the above two forms:

the approximate solution under the special pressure distribution of hydraulic fracture coincides with the accurate solution very well, especially in the center of the fracture half-length (near the well results of the approximate solution are slightly larger than results of the accurate solution, near the fracture tip the results are just the opposite slightly lower). Fig. 17 shows that the greatest relative error of the approximate solution is about 4%. Errors of this magnitude in the engineering calculation are acceptable.

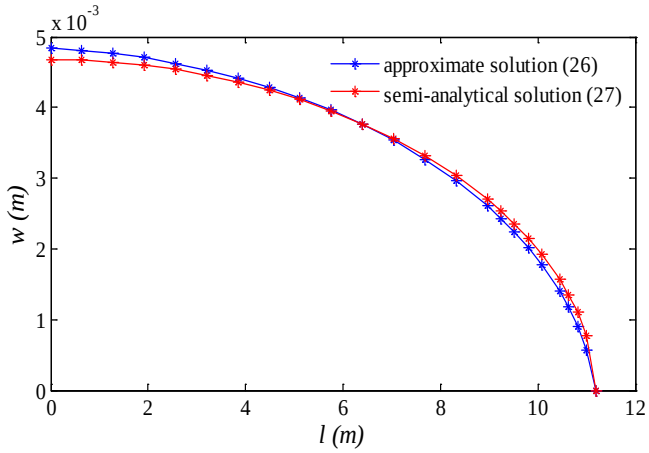

Fig. 14. The fracture openings from the approximate and semi-analytical solutions under

$$t=30\ s,\ \ l=11.2\,m$$

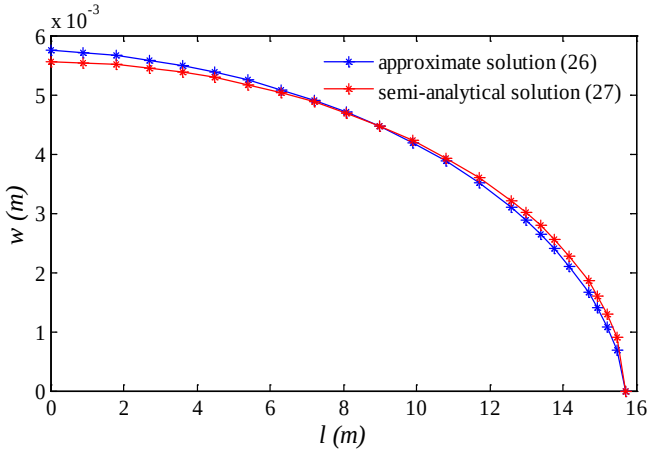

Fig. 15. The fracture openings from the approximate and semi-analytical solutions under

$$t=50\ s,\ \ l=15.7\,m$$

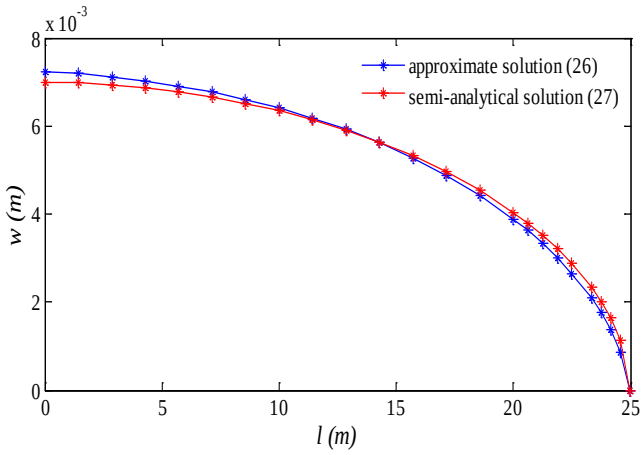

Fig. 16. The fracture openings from the approximate and semi-analytical solutions under t=100 s, $l = 25.0\,m$

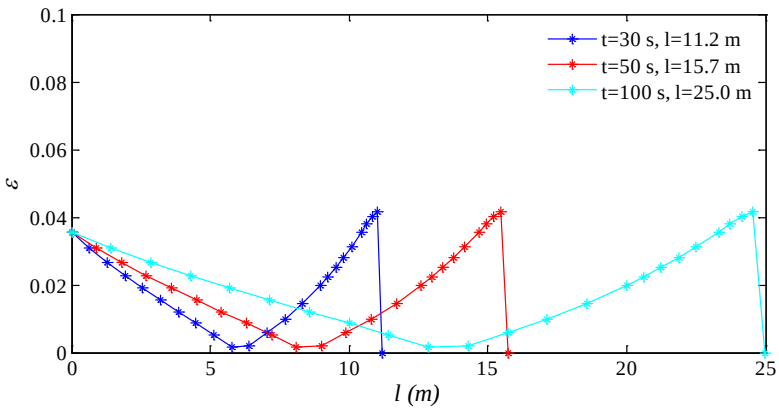

Fig.17. The relative errors of the above three different pressure distributions in Fig. 5

5. Conclusions

The approximate solution developed in this paper has a small relative error, as compared with the exact solution for the actual fracture opening. In the engineering calculation, this error can be neglected. It means that approximate solution can be used instead of the semi-analytical solution in numerical simulations of hydraulic fracturing. The developed solution has the following advantages as compared with the exact one:

(1) It is an explicit analytical solution that differs from the semi-analytical solution, which is an integral expression of the fluid pressure and cannot be directly substituted into the fluid continuity equation. The approximate solution can be directly substituted into the continuity equation to simplify the solving process at each step.

(2) Application of the developed analytical solution reduces essentially a time for calculation process as compared with the discontinuous displacements method of numerical simulation for hydraulic fracturing modeling, which requires iterations and grid refinement to obtain relatively precise numerical results.

Acknowledgments. *This work is supported in parts by RFBR grant No.18-07-00513, and by China Schoolship Council and Education Department of Chinese Embassy in Russia.*

References

[1] Perkins TK, Kern LR. Widths of hydraulic fractures. *J. Petrol. Technol.* 1961;13(9): 937-949.

[2] Nordgren RP. Propagation of vertical hydraulic fractures. *Soc. Petrol. Eng. Journal*. 1972;12(4): 306-314.

[3] Kristianovich SA, Zheltov YP. Formation of vertical fractures by means of highly viscous Fluids. In: *Proceedings of the 4th World Petroleum Congress.* Rome, Italy: 1955. p.579-586.

[4] Geertsma J, de Klerk F. A rapid method of predicting width and extent of hydraulic induced fractures. *Journal of Petroleum Technology*. 1969;21(12): 1571-1581.

[5] Sneddon IN, Lowengrub M. *Crack problems in the classical theory of elasticity*. New York: John Wiley & Sons; 1969.

[6] Crouch SL. Solution of plane elasticity problems by the displacement discontinuity method. *International Journal for Numerical Methods in Engineering*. 1976;10(2): 301-343.

[7] Detournay E. Propagation regimes of fluid-driven fractures in impermeable rocks. *International Journal of Geomechanics.* 2004;4(1): 35-45.

[8] Garagash DI. Plane-strain propagation of a fluid-driven fracture during injection and shut-in: asymptotics of large toughness. *Engineering Fracture Mechanics*. 2006;73(4): 456-481.

[9] Garagash DI. Propagation of a plane-strain hydraulic fracture with a fluid lag: early-time solution. *International Journal of Solids and Structures*. 2006;43(18-19): 5811-5835.

[10] Lecampion B, Detournay E. An implicit algorithm for the propagation of a hydraulic fracture with a uid lag. *Comput. Methods Appl. Mech. Engrg.* 2007;196(49-52): 4863-4880.

[11] Chekhonin E, Levonyan K. Hydraulic fracture propagation in highly permeable formations, with applications to tip screenout. *International Journal of Rock Mechanics & Mining Sciences*. 2012;50: 19-28.

[12] Sesetty V, Ghassemi A. A numerical study of sequential and simultaneous hydraulic fracturing in single and multi-lateral horizontal wells. *Journal of Petroleum Science and Engineering.* 2015;132: 65-76.

[13] Linmao X, Ki-Bok Min, Baotang S. Simulation of hydraulic fracturing and its interactions with a preexisting fracture using displacement discontinuity method. *Journal of Natural Gas Science and Engineering*. 2016;36: 1284-1294.

[14] Ren L, Su Y, Zhan S, Hao Y, Meng F, Sheng G. Modeling and simulation of complex fracture network propagation with SRV fracturing in unconventional shale reservoirs. *Journal of Natural Gas Science and Engineering.* 2016;28: 132-141.

[15] Yun X, Ming C, Qi W, Deqi L, Nengyu Y, Dingwei W, Baoshan G. Stress interference calculation model and its application in volume stimulation of horizontal wells. *Petroleum Exploration and Development.* 2016;43(5): 849-856.

[16] Chen X, Li Y, Zhao J, Xu W, Fu D. Numerical investigation for simultaneous growth of hydraulic fractures in multiple horizontal wells. *Journal of Natural Gas Science and Engineering.* 2018;51: 44-52.

[17] Desroches J, Detournay E, Lenoach B, Papanastasiou P, Pearson JRA, Thiercelin M, Cheng A. The crack tip region in hydraulic fracturing. *Mathematical and Physical Sciences.* 1994;447(1929): 39-48.

[18] Garagash D, Detournay E. The tip region of a fluid-driven fracture in an elastic medium.

Journal of applied mechanics. 2000;67(1): 183-192.
[19] Detournay E. Propagation Regimes of Fluid-Driven Fractures in Impermeable Rocks. *Int. J. Geomech.* 2004;4(1): 35-45.
[20] Garagash D, Detournay E. Plane-strain propagation of a fluid-driven fracture: small toughness solution. *Journal of Applied Mechanics.* 2005;72(6): 916-928.
[21] Dontsov EV, Peirce AP. Comparison of toughness propagation criteria for blade-like and pseudo-3D hydraulic fractures. *Engineering Fracture Mechanics*. 2016;160: 238-247.
[22] Spence DA, Sharp P. Self-similar solutions for elastohydrodynamic cavity flow. *Proc. R. Soc. London, Ser. A.* 1985:400(1819): 289-313.